AIP Advances

Extensive study of magneto-optical and optical properties of $Cd_{1-x}Mn_xTe$ between 675 and 1025 nm

Cite as: AIP Advances **13**, 015213 (2023); https://doi.org/10.1063/5.0130535
Submitted: 12 December 2022 • Accepted: 16 December 2022 • Published Online: 13 January 2023

Christoph Tyborski, Muhammad T. Hassan, Thomas Flisgen, et al.

Extensive study of magneto-optical and optical properties of $Cd_{1-x}Mn_xTe$ between 675 and 1025 nm

Cite as: AIP Advances 13, 015213 (2023); doi: 10.1063/5.0130535
Submitted: 12 December 2022 • Accepted: 16 December 2022 •
Published Online: 13 January 2023

Christoph Tyborski,[a] Muhammad T. Hassan, Thomas Flisgen, Max Schiemangk, and Andreas Wicht[b]

AFFILIATIONS

Ferdinand-Braun-Institut gGmbH, Leibniz-Institut für Höchstfrequenztechnik, Gustav-Kirchhoff-Str. 4, 12489 Berlin, Germany

[a]Author to whom correspondence should be addressed: Christoph.Tyborski@fbh-berlin.de
[b]Electronic mail: Andreas.Wicht@fbh-berlin.de

ABSTRACT

We determine Faraday rotations and measure the optical reflection and transmission from magneto-optical $Cd_{1-x}Mn_xTe$ crystals with various stoichiometric ratios. For wavelengths between 675 and 1025 nm, we derive Verdet constants, optical loss coefficients, and the complex indices of reflection that are relevant measures to find suitable stoichiometric ratios of $Cd_{1-x}Mn_xTe$ for the realization of miniaturized optical isolators. By reflection and transmission measurements, we determine the stoichiometric ratios of several different $Cd_{1-x}Mn_xTe$ crystals and discuss the observed dependence of the optical properties on the stoichiometric ratio with respect to their use in optical isolators. Finally, we show the relevant figure of merit, i.e., the ratio of Verdet constants and optical loss coefficients for $Cd_{1-x}Mn_xTe$ crystals with Mn contents ranging from $x = 0.14$ to $x = 0.50$.

I. INTRODUCTION

Due to a wide field of possible applications such as optical clocks, atom-interferometry-based accelerometers, or (coherent) free-space laser communication, the demand for very compact laser systems increased in the last decade.[1–3] Small form factors can be realized with diode laser-based approaches covering a wavelength range from 237 nm (AlGaN) up to several μm (GaSb)[4–8] when III–V semiconducting materials are used. However, applications like strontium-based optical clocks[9,10] or the preparation of Bose–Einstein–Condensates in microgravity[1,2] only require a smaller wavelength range that can be addressed by GaAs-based laser diodes (626–1128 nm).[11–14]

One indispensable component for the reliable operation of a diode-based laser is an optical isolator that protects the laser against optical feedback. Commercially available miniaturized optical isolators, based on the Faraday effect, are only suitable for the wavelength ranges of 770–810 nm and 1040–1090 nm or are only available for discrete wavelengths such as 852, 690, or 633 nm, thus limiting the use of GaAs-based lasers for the state-of-the-art applications.[15–18] The availability of miniaturized optical isolators with volumes smaller than 1 ml is even more limited. Up to today, miniaturized optical isolators especially for shorter wavelengths are still commercially not available. The reason is mainly the lack of a proper magneto-optical material with a sufficiently large Verdet constant and/or of magnets with a sufficiently large remanence field. Consequently, Faraday rotations of 45° necessary to realize an optical isolator cannot be realized in a miniature setup based on readily available materials.[19,20]

One possible magneto-optical material suitable to fill this gap is $Cd_{1-x}Mn_xTe$.[21–23] By a defined addition of manganese to CdTe, both the bandgap and the wavelength-dependent Verdet constant can be tuned within a range of 1.5–2.2 eV (827–564 nm), limited by a dominant Mn^{++} intra-ion transition for higher photon energies.[21,22,24–26] Hence, the addition of Mn principally allows for the optimization of the alloy to a specific wavelength.

Although the Verdet constants for some stoichiometric ratios of $Cd_{1-x}Mn_xTe$ and some wavelengths are given in the literature, a

detailed and extensive analysis of both, Verdet constants and optical loss coefficients, is still not available. However, an assessment of both quantities is a necessity to decide if $Cd_{1-x}Mn_xTe$ with a proper stoichiometric ratio can be used to realize miniaturized optical isolators for a required wavelength.

In this article, we experimentally determine the Verdet constants and optical loss coefficients for four stoichiometric ratios of $Cd_{1-x}Mn_xTe$: $x = 0.14$, $x = 0.25$, $x = 0.43$, and $x = 0.5$ between 675 and 1025 nm. From reflection/transmission measurements, we derive the wavelength-dependent complex index of refraction $\mathbf{n} = n - i\kappa$, i.e., the index of refraction n and the extinction coefficient κ for all crystals. Furthermore, we determine the absorption edges of several $Cd_{1-x}Mn_xTe$ crystals with nominal Mn contents of 14% and 25% and derive the corresponding stoichiometric ratios differing significantly from their nominal values given by the manufacturer. We discuss these discrepancies and relate this aspect to the characteristics of the crystal growing process. We show the relevant figure of merit, i.e., the ratio of Verdet constant and optical loss coefficient, and calculate crystal-induced optical losses between 675 and 1025 nm when $Cd_{1-x}Mn_xTe$ crystals are used as a Faraday rotator in a miniaturized optical isolator.

II. EXPERIMENTAL DETAILS

Eleven $Cd_{1-x}Mn_xTe$ crystals have been procured from International Crystals Laboratories with dimensions smaller than $1.8 \times 1.8 \times 2.0$ mm^3. For all of the crystals, the front and rear facets are polished with optical quality. Four of them (2× $Cd_{0.86}Mn_{0.14}Te$ and 2× $Cd_{0.75}Mn_{0.25}Te$) are anti-reflection coated for 770–960 and 780 nm, respectively. A list of the measured crystals can be seen in Table I.

The optical measurements were conducted with a Matisse CR Ti:Sa laser from Sirah. Emitted wavelengths were determined with absolute accuracies of ±0.1 nm. Laser powers were kept at 30 mW for all measurements to avoid thermo-optical changes in the optical response from the crystals and to reduce the influence of nonlinearities of the used power detectors. A collimated beam with a focal beam diameter $(1/e^2)$ of 600 μm was used for all measurements, and each crystal was placed within the Rayleigh range of the beam. At all times, the ambient temperature was kept at T = 295 ± 2 K. Schematics of the experimental setups are shown in Fig. 1.

To extract the normalized reflection/transmission from the reflection/transmission measurements [$R^{exp.}$ and $T^{exp.}$ in Fig. 1(a)],

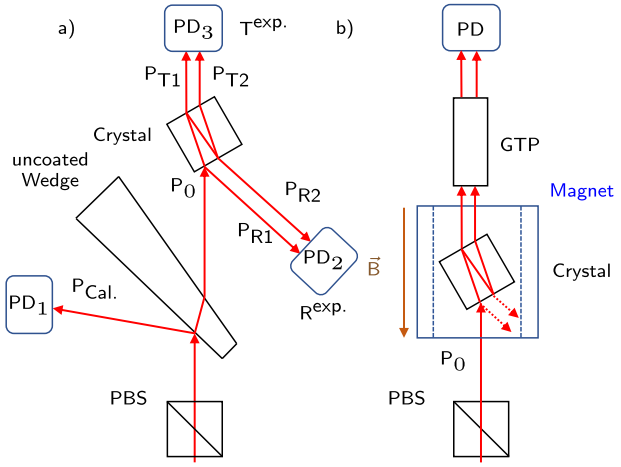

FIG. 1. Schematic setups for measurements of the reflection/transmission values (a) and the Verdet constants (b) of $Cd_{1-x}Mn_xTe$ crystals. Red arrows indicate the propagation direction of the light. $P_{Cal.}$, P_R, and P_T stand for calibration, reflected, and transmitted power, respectively. $R^{exp.}$ and $T^{exp.}$ stand for experimentally recorded, reflected and transmitted power both including two contributions $P_{R1} + P_{R2}$ and $P_{T1} + P_{T2}$, respectively. PD, PBS, and GTP stand for power detector, polarizing beamsplitter cube, and Glan–Thompson–Prism, respectively. $\vec{B}$ indicates the direction of the magnetic field inside the magnet. Note that the scaling does not correspond to the actual sizes of components.

we calibrated two pairs of power detectors (Thorlabs S130C), namely, PD_1 to PD_3 and PD_2 to PD_3 [see Fig. 1(a)]. The calibrations are necessary to account for the wavelength-dependent reflection/transmission ratios of the uncoated wedge, to eliminate absolute measurement uncertainties, and to account for the different spectrally dependent sensitivities of different power detectors. The remaining measuring uncertainty of the normalized reflection and transmission originates from the power dependence of ±0.5% from the power detector PD_3 [see Fig. 1(a)], resulting in a total measuring uncertainty of ±1%. One pair of calibrated power detectors was only used for reflection, and one pair was only used for the transmission measurements. With these calibrations, the setup allows for a simultaneous measurement of the relative transmission and reflection of the $Cd_{1-x}Mn_xTe$ crystals as the laser frequency is swept. The apparatus was set up such that we measure the lumped power of two

TABLE I. An overview of the measured $Cd_{1-x}Mn_xTe$ crystals with the nominal and experimentally determined Mn concentration and their optical loss coefficients for $\lambda = 800$ nm is given. Crystals marked with an asterisk are anti-reflection coated. Note that the optical loss coefficients also include coating-induced losses. The exp. determined Mn concentrations are derived from absorption measurements following Ref. 27.

Amount	Nom. Mn concentration	Expt. determined Mn concentration	Optical loss coefficient at 800 nm (mm^{-1})
2	$Cd_{0.86}Mn_{0.14}Te^*$ (14% Mn)	15.5% Mn–15.8%Mn	0.164–0.166
2	$Cd_{0.86}Mn_{0.14}Te$ (14% Mn)	16.5% Mn–16.8%Mn	0.118–0.241
3	$Cd_{0.75}Mn_{0.25}Te^*$ (25% Mn)	~21% Mn	0.111–0.117
2	$Cd_{0.57}Mn_{0.43}Te$ (43% Mn)	···	0.128–0.226
2	$Cd_{0.50}Mn_{0.50}Te$ (50% Mn)	···	0.169–0.171

beams reflected from the crystals [P_{R1} and P_{R2} in Fig. 1(a)] and two beams transmitted through the crystals [P_{T1} and P_{T2} in Fig. 1(a)]. Each crystal was tilted with respect to the incident beam such that the angle of incidence (AOI) is 30° with respect to the geometrical axis of the crystal. This ensures that the multiple beams that are created by multiple reflections at the facets are spatially separated but are not clipped, and interference on the power detector is avoided.

For the measurement of the Verdet constants, the crystals were placed into a magnet with a known magnetic field. The combination of crystal length, its position, and the specific field of the magnet results in an integrated field of $\int_0^{L_{eff.}} dz\, B_z(z) \approx -0.85$ T mm, where $L_{eff.}$ is the effective optical length and z is the propagation direction of the beam within the analyzed crystals. For each crystal, the (wavelength-dependent) integrated field was calculated individually. The Faraday rotation was measured with a Glan–Thompson–Prism (GTP) mounted in a rotation stage between rotation angles of 0° and 720° for each run. Resulting intensity graphs were then fitted with $\sin^2(\Theta)$ functions. In the first run, a calibration measurement without a crystal was calculated to obtain the offset angle of the GTP with respect to the input polarizing beamsplitter cube (PBS). All following measurements of the Faraday rotation are referenced to that offset angle, see Fig. 2(a).

III. RESULTS

A. Verdet constants

From the measured Faraday rotations $\Theta(\lambda)$, we derive the wavelength-dependent Verdet constants via

$$V(\lambda) = \frac{\Theta(\lambda)}{\int_0^{L_{eff.}(\lambda)} dz B_z(z)}, \quad (1)$$

as shown in Fig. 2(a). One should note that the tilting angle of the crystals [compare Fig. 1(b)] leads to a reduction of the effective propagation length of the beam along the magnetic field lines inside the magnet. We have calculated the effective length via

$$L_{eff.}(\lambda) = L \cdot \frac{\cos[\,AOI - \beta(n(\lambda))]}{\cos[\beta(n(\lambda))]}, \quad (2)$$

where AOI denotes the angle of incidence onto the facet, $\beta(n)$ is the angle of refraction, and L is the length of the crystal. Values for the refractive index are taken from Ref. 27. The experimentally determined refractive indices from the reflection and transmission measurements were not used for the calculation of $L_{eff.}$ as they deviate from the literature values (discussed in Sec. III B). Furthermore, it should be noted that we measure the optical power of two transmitted beams: The directly transmitted beam and a second beam generated by two consecutive reflections: first at the rear facet and then at the front facet. The latter exhibits three times the Faraday rotation compared to the direct path, thus exhibiting a different rotation. However, its power in the case of $Cd_{0.57}Mn_{0.43}Te$ and $Cd_{0.50}Mn_{0.50}Te$ ranges between 0.5% and 2%, and for $Cd_{0.86}Mn_{0.14}Te$, its power is in the range of 2%. For the coated crystals, the relative power is even smaller by two orders of magnitudes. Hence, the optical power of beams created by parasitic reflections at the facets can be neglected.

In accordance with former findings reported in the literature,[22–24,26,28] we observe the Verdet constants with a negative sign for the investigated wavelengths. The Mn content in the analyzed crystals (14%–50%) causes a pronounced *sp–d* exchange interaction that leads to an enhanced spin splitting of electronic states close to the band edges when applied to a magnetic field.[21,22] The resulting enhanced Zeeman splitting dominates over the intrinsic g-factors of charge carriers in the valence and

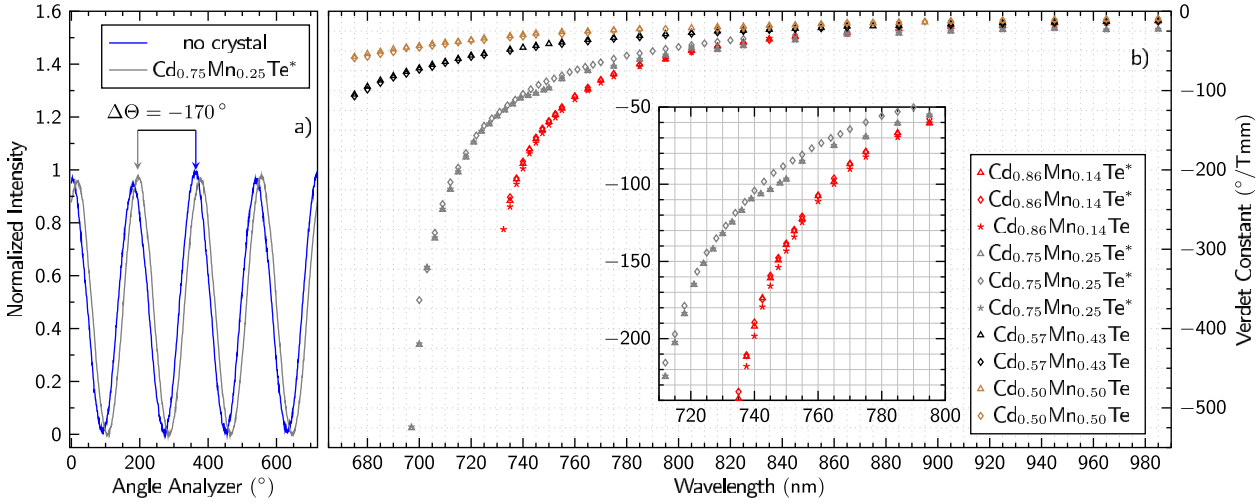

FIG. 2. (a) The Faraday rotation observed for a $Cd_{0.75}Mn_{0.25}Te$ crystal (L = 1.7 mm) for λ = 715 nm is shown. The magneto-optic effect together with the magnetic field orientation, as indicated in Fig. 1(b), causes a polarization rotation of $\Theta = -170°$ in reference to a measurement without a $Cd_{1-x}Mn_xTe$ crystal. Note that $Cd_{1-x}Mn_xTe$ has a negative Verdet constant and, thus, causes a negative Faraday rotation in the experimental setup, as shown in Fig. 1(b). (b) The wavelength-dependent Verdet constants of different crystals with different stoichiometric ratios are plotted. Note that the ratios given are those communicated from the manufacturer and deviate from the experimentally determined ratios. Crystals denoted with an asterisk are anti-reflection coated. The ambient temperature is T = 295 ± 2 K.

conduction bands and induces a large circular birefringence that is responsible for the large Faraday rotation with a negative sign.[21,22] The effect scales with the photon energies in a way that the circular birefringence and, therefore, the absolute value of the Verdet constants increase when the photon energies approach the bandgap energy. For $Cd_{0.86}Mn_{0.14}Te$ and $Cd_{0.75}Mn_{0.25}Te$, we find the Verdet constants of several hundred °/T mm close to the band edges [Fig. 2(b)]. The largest absolute values of the Verdet constant have been measured for $Cd_{0.75}Mn_{0.25}Te$ as the Mn-induced *sp–d* interaction; therefore, the Zeeman splitting is larger than for $Cd_{0.86}Mn_{0.14}Te$.[21,22]

We also find that the Verdet constants of nominally identical crystals differ. For the design of an optical isolator, this aspect is very important and is discussed at the end of Sec. III B.

B. Optical loss coefficient, complex refractive index, and stoichiometric ratio

To obtain the optical loss coefficients of single $Cd_{1-x}Mn_xTe$ crystals, we performed reflection and transmission measurements for a wavelength range of 675–1025 nm. An example of the result of such a measurement for two polished crystals ($Cd_{0.86}Mn_{0.14}Te$ and $Cd_{0.57}Mn_{0.43}Te$) is shown in Fig. 3(a). Data of the remaining crystals can be found in the supplementary material. Note that the transmission and reflection values contain contributions from both direct reflections/transmissions and contributions, which arise due to parasitic reflections at the facets as already described above.

From the experimentally obtained reflection and transmission [$R^{exp.}$, $T^{exp.}$ in Fig. 1(b)], we calculate the normalized transmission and reflection (as shown in Fig. 3) and derive the reflectance R and optical loss coefficients α' numerically by solving the following system of equations:

$$R^{exp.}_{normalized} = P_0 \cdot \left[R + (1-R)^2 \cdot R \cdot e^{-2\alpha' \cdot L'(n)}\right], \quad (3)$$

$$T^{exp.}_{normalized} = P_0 \cdot \left[(1-R)^2 \cdot e^{-\alpha' \cdot L'(n)} + (1-R)^2 \cdot R^2 \cdot e^{-3\alpha' \cdot L'(n)}\right], \quad (4)$$

where the first summand in each outer parenthesis accounts for the direct reflection/transmission paths [corresponding to P_{R1} and P_{T1} in Fig. 1(a)], and the second summand accounts for reflection/transmission paths with internal reflections [P_{R2} and P_{T2} in Fig. 1(a)]. The optical path length $L'(n)$ inside the crystals depends on the angle of incidence (AOI = 30°) and the refractive index n according to: $L' = L \cdot \sqrt{1 + (\sin(30° \cdot \frac{n_{CdMnTe}}{n_{Air}}))^2}$. The optical path lengths were calculated individually for each stoichiometric ratio and wavelength with refractive indices taken from Ref. 27. The values of the optical loss coefficient α' are given in Figs. 3(b) and 3(c).

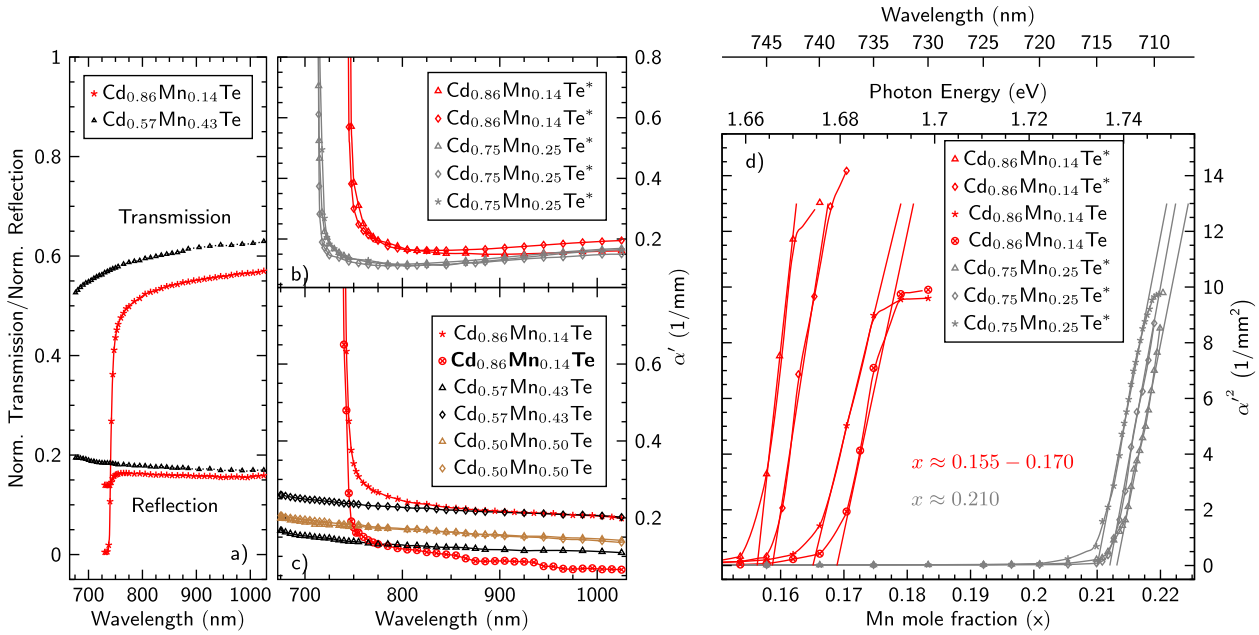

FIG. 3. (a) Normalized, wavelength-dependent reflection and transmission graphs for an angle of incidence of 30° are shown for $Cd_{1-x}Mn_xTe$ with $x = 0.14$ and $x = 0.43$, respectively. (b) and (c) Wavelength-dependent optical loss coefficients for $Cd_{1-x}Mn_xTe$ crystals with four different stoichiometric ratios are plotted. (d) The square of the optical loss coefficient (α'^2) is plotted as a function of the photon energy (top x axis). With a linear regression, one can find the stoichiometric ratio of the analyzed crystals. Values at the bottom x axis are converted from the photon energies as given on the top x axis following Ref. 27. Note that the stoichiometric ratios given in the legend correspond to values provided by the manufacturer and deviate from the experimentally determined ratios. Crystals denoted with an asterisk are anti-reflection coated. Experimental reflection and transmission data of one $Cd_{0.86}Mn_{0.14}Te$ crystal in (c) (bold, denoted with a circled cross) are used to determine the complex refractive index, as shown in Fig. 4. The ambient temperature is T = 295 ± 2 K. Lines are a guide to the eye.

It should be noted that we solve Eqs. (3) and (4) under the assumption that the reflectivities at the front and rear facets of the crystals are equal. In particular, this is not the case as the growth process of $Cd_{1-x}Mn_xTe$ crystals leads to a Mn-gradient between the first-to-freeze and the end-to-freeze region of a few 0.1% over centimeters.[29–31] Differences of the Fresnel reflectivities resulting from this gradient are on the order of only $\approx 10^{-5}$ and hence can be neglected.[27] It is further important to note that experimentally obtained Verdet constants and loss coefficients constitute values that are averaged over the volume of the crystals, sampled by the optical beam. Therefore, the Mn-gradient within the crystals limits the experimental sensitivity to an (over the volume of the analyzed crystals) averaged Verdet constant and an averaged optical loss coefficient.

For the uncoated crystals, we observe smaller optical loss coefficients for longer wavelengths with values in the range of 0.25 mm^{-1} and less, see Fig. 3(c). In contrast, the optical loss coefficients for the coated crystals increase for larger wavelengths, see Fig. 3(b). We attribute this finding to additional losses introduced by the anti-reflection coating. Variations of the loss coefficients can be explained by Te inclusions that constitute scattering centers in the bulk material. They differ with respect to their amount and size and cause variations independent from the actual bandgap.[32–34] It is important to note that different origins of optical losses cannot be separated by the conducted measurements. As mentioned above, optical losses can occur due to coating-induced losses, scattering at Te inclusions, and the bulk absorption from $Cd_{1-x}Mn_xTe$.

To get more insights into the optical properties of the analyzed crystals, we deduce the complex refractive index, i.e., n and κ from the reflection/transmission measurements carried out on the uncoated crystals. To that end, we have solved the equation system consisting of Eqs. (3) and (4) with the substitutions

$$\alpha = \frac{4\pi\kappa}{\lambda}, \tag{5}$$

$$R = \left| \frac{(n + i\kappa)\cos(\mathrm{AOI}) - \frac{\sqrt{(n+i\kappa)^2 - \sin(\mathrm{AOI})^2}}{(n+i\kappa)}}{(n + i\kappa)\cos(\mathrm{AOI}) + \frac{\sqrt{(n+i\kappa)^2 - \sin(\mathrm{AOI})^2}}{(n+i\kappa)}} \right|^2, \tag{6}$$

where α denotes the bulk optical absorption. We have only solved the equations for the uncoated crystals; otherwise, the deduction of n and κ would lead to odd values. Values obtained for n and κ are shown for one crystal ($Cd_{0.86}Mn_{0.14}Te$) as an example in Fig. 4.

Only for this specific crystal sample, we find good agreement between the experimentally determined wavelength-dependent refractive index and values given in the literature[27] (see also supplementary material). It is important to note that this crystal exhibits the lowest optical loss coefficient α' among all other crystals (Fig. 3). The observed agreement is explained as follows: The physical model behind the absorption coefficient α [Eq. (5)] and the reflectivity R [Eq. (6)] assumes a homogeneous bulk material, the optical properties of which can be described by only wavelength-dependent, complex-valued index of refraction $\mathbf{n} = n + i\kappa$.

However, for $Cd_{1-x}Mn_xTe$ crystals, this assumption is not justified as they often exhibit Te inclusions with large densities of $\cong 10^4$–10^5 cm^{-3} and particle sizes between 5 and 20 μm.[29,33] The Te inclusions constitute scattering centers that alter the measured transmission and reflection in comparison to $Cd_{1-x}Mn_xTe$ free of Te inclusions in a way that cannot be described by n and κ only. We observe the largest deviations of the measured refractive index n and corresponding values from the literature[27] for those crystals that show the highest optical losses and vice versa (see also supplementary material).

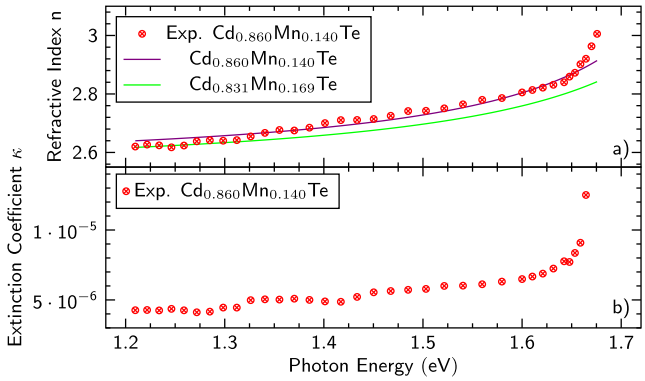

FIG. 4. Experimentally determined wavelength-dependent refractive index n and extinction coefficient κ for one $Cd_{0.86}Mn_{0.14}Te$ crystal sample are shown. The specific crystal exhibits the lowest optical losses and is denoted in bold letters in Fig. 3(c). For comparison, the refractive indices calculated[27] for $Cd_{0.860}Mn_{0.140}Te$ and $Cd_{0.831}Mn_{0.169}Te$ are plotted that correspond to the crystals with the nominal and the experimentally determined stoichiometric ratios, respectively. The ambient temperature was T = 295 ± 2 K.

Following that argumentation, the conducted measurements indicate that, due to the good agreement of the experimentally determined refractive index and values from the literature,[27] the optical loss of the specific $Cd_{0.86}Mn_{0.14}Te$ crystal, as shown in Fig. 4, is rather caused by the bulk absorption than by scattering at Te inclusions. Moreover, the good agreement and the low optical loss coefficient might also indicate that the intrinsic absorption level for that specific crystal is reached, exhibiting ≤ 0.1 mm^{-1} in the transparent regime [see Fig. 3(c)].

To assess the accuracy of the stoichiometric ratios provided by the supplier, we have also determined the stoichiometric ratios of the available samples from our measurement data. We assume that the optical loss α' for photon energies very close to the bandgap is dominated by the intrinsic absorption α rather than by scattering at Te inclusions, i.e., $\alpha \approx \alpha'$. The bandgap energy can then be derived from the spectrally resolved loss coefficients α' [Figs. 3(b) and 3(c)] when proper models for the dependence of the bandgap energy on photon energy are applied.[21,35]

$Cd_{1-x}Mn_xTe$ is a direct semiconductor in which the optical absorption α follows a square root gradient dependence as a function of the photon energy.[21,35] Thus, by plotting the square of the optical loss coefficients α', one can fit the experimentally determined absorption coefficient with a linear regression of the transmission decay, as shown in Fig. 3(d).[35] The lower x axis in Fig. 3(d) can be used to directly read off the Mn content from the analyzed crystals and is scaled according to Ref. 28. There are also other expressions on how the Mn content changes the bandgap of diluted $Cd_{1-x}Mn_xTe$ to be found in the literature.[36,37] The different models predict slightly different Mn contents of $x \approx 0.12$–0.14 ($Cd_{0.86}Mn_{0.14}Te$) and

$x \approx 0.178$ ($Cd_{0.75}Mn_{0.25}Te$)[36] as well as Mn contents of $x \approx 0.105$ –0.115 ($Cd_{0.86}Mn_{0.14}Te$) and $x \approx 0.16$ ($Cd_{0.75}Mn_{0.25}Te$)[37] with the nominal stoichiometric ratios provided by the manufacturer given in parenthesis. Five different measurements of the transmission and reflection for one $Cd_{0.86}Mn_{0.14}Te$ crystal showed that the band edges could be determined within an energy range of $\Delta E \approx 10$ meV that corresponds to a range of Mn content $\Delta x \approx 0.005$.

We can make two observations: (*i*) Experimentally determined stoichiometric ratios deviate from the nominal ones by several percentage points. (*ii*) Mn content variations of several 0.5% points can be found for crystals nominally exhibiting identical stoichiometric ratios.

All observations can be related to growth-induced axial and lateral Mn gradients in $Cd_{1-x}Mn_xTe$ ingots caused by the Mn segregation coefficient being less than a unit.[29–31] Hence, even crystals taken from the same ingot will exhibit slightly different Mn contents and, therefore, display slightly different optical and magneto-optical properties.

For the design of an optical isolator, the knowledge of the exact Mn content is crucial. The selection of the optimum Mn content results from a trade-off between maximizing the Verdet constant and minimizing the transmission loss. As a result of this optimization, the photon energy at the operating wavelength typically is close to the bandgap energy. Hence, even small variations of the Mn content may strongly affect the loss coefficient as well as the Verdet constant.

C. Figure of merit

The knowledge of both the Verdet constant and the optical loss coefficient can be used to evaluate the ratio $V(\lambda)/\alpha'(\lambda)$, which provides a figure of merit suitable to describe the optical and magneto-optical performance of a given crystal as a Faraday rotator. This figure of merit is given in Fig. 5(a).

For all stoichiometric ratios, the absolute values of the figure of merit increase when photon energies approach the bandgap and decrease quickly when the bulk absorption begins. The highest absolute values close to 1000 °/T are reached for $Cd_{0.75}Mn_{0.25}Te$. Experimentally observed variations of the figure of merit for crystals with nominally identical stoichiometric ratios originate from variations in the optical loss coefficients rather than from changes in the Verdet constants. Following the argumentation given above, the dashed line in Fig. 5(a) corresponds to the figure of merit of $Cd_{0.86}Mn_{0.14}Te$ (14% nominal Mn content) crystals with negligible Te inclusions.

In comparison to other common magneto-optical materials such as TGG (Terbium Gallium Garnet) or TSAG (Terbium Scandium Aluminum Garnet), the absolute values observed for the $Cd_{1-x}Mn_xTe$ samples are at least one order of magnitude smaller.[38–40] Due to the comparably small Verdet constants of TGG and TSAG, these magneto-optical materials are, however, unsuitable for very compact optical isolators.

Crystal lengths of $Cd_{1-x}Mn_xTe$ required for the fabrication of miniaturized optical isolators are shown in Fig. 5(b). Lengths were calculated for a Faraday rotation of $\Theta = 45°$ and a magnetic field of 0.55 T. The latter can be reached with FeNdB magnets exhibiting volumes below 0.5 cm^3. For each wavelength-dependent crystal length, a corresponding optical loss is given. Assuming a tolerable optical loss of 1.5 dB (≈29.2%), a wavelength range from 675 to 925 nm can be covered with $Cd_{1-x}Mn_xTe$ crystals exhibiting Mn contents between 14% and 50% Te. In case, a higher loss of 3 dB (≈50.1%) is accepted, the wavelength range between 675 and 1025 nm can be covered.

IV. CONCLUSION

In this paper, we reported the Verdet constants and the optical loss coefficients for various $Cd_{1-x}Mn_xTe$ crystals with Mn contents

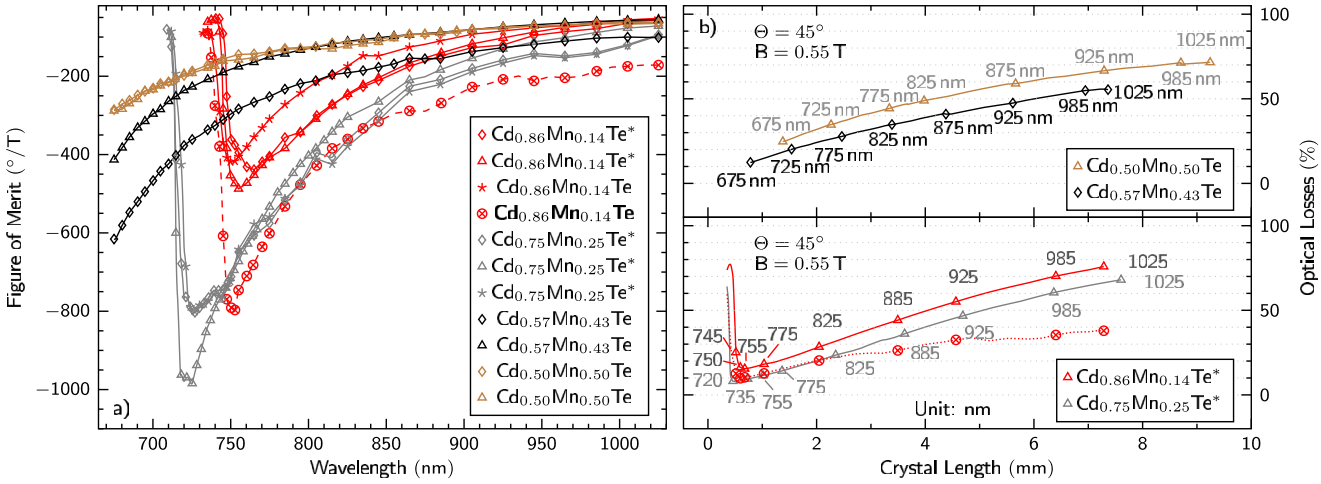

FIG. 5. (a) The wavelength-dependent figure of merit $[V(\lambda)/\alpha'(\lambda)]$ for four stoichiometric ratios of $Cd_{1-x}Mn_xTe$ is shown. The $Cd_{0.86}Mn_{0.14}Te$ crystal denoted with a dashed line exhibits the lowest optical losses among all analyzed crystals. Experimentally obtained values for n and κ can be found in Fig. 4. (b) Crystal-induced optical losses for $Cd_{1-x}Mn_xTe$ crystal lengths necessary to reach a Faraday rotation of $\Theta = 45°$ for many wavelengths are shown. The considered magnetic field of B = 0.55 T can be reached by a magnet with a volume smaller than 0.5 cm^3. Crystals denoted with an asterisk are anti-reflection coated. All lines are a guide to the eye. The ambient temperature is T = 295 ± 2 K.

of 14%, 25%, 43%, and 50% for a wavelength range between 675 and 1025 nm. Depending on the Mn content, we find the Verdet constants of several hundred negative °/T mm close to the band edges. At wavelengths with photon energies below the bandgap energies, the Verdet constants are fairly independent of wavelength and Mn contents. The same is found for the optical loss coefficients exhibiting 0.05–0.25 mm^{-1}. Any potential dependence of the optical loss coefficient on the Mn content is masked by variations of the optical loss coefficient due to Te inclusions, which vary considerably between different samples. For one of the $Cd_{0.86}Mn_{0.14}Te$ crystal samples, we experimentally determine an optical loss coefficient of only 0.07–0.1 mm^{-1}. For this crystal, we find the wavelength-dependent refractive index n and extinction coefficient κ to be in good agreement with values reported in the literature. This finding is consistent with assuming that this specific sample, in contrast to the other samples that we investigated, exhibits very small scattering induced by Te inclusions. Hence, the loss coefficient determined for this sample reflects the unavoidable bulk loss for $Cd_{0.86}Mn_{0.14}Te$.

From both the Verdet constant and the optical loss coefficient, we determine the figure of merit for all $Cd_{1-x}Mn_xTe$ crystals between 675 and 1025 nm and report values of close to −1000°/T for $Cd_{0.75}Mn_{0.25}Te$ around 720 nm. Based on our data, we determine the optical losses of the bulk material for crystals that provide 45° of Faraday rotation as a requirement for the use in miniaturized optical isolators with volumes of 0.5 mm^3. Assuming an acceptable loss of 1.5 dB (≈29.2%), a wavelength range of 675 up to 925 nm can be covered with crystals that feature a Mn content between 14% and 50%. Hence, we conclude that $Cd_{1-x}Mn_xTe$ is a magneto-optical material with great potential for compact lasers based on GaAs laser diodes.

SUPPLEMENTARY MATERIAL

See supplementary material for the normalized, wavelength-dependent transmission and reflection data and the derived values of the wavelength-dependent refractive index n and extinction coefficient κ from the investigated $Cd_{1-x}Mn_xTe$ crystals.

ACKNOWLEDGMENTS

The authors acknowledge financial support by the VDI Technologiezentrum GmbH with funds provided by the Federal Ministry of Education and Research (BMBF) under Grant Nos. 13N14906 and 13N15724 and by the DLR Space Administration with funds provided by the Federal Ministry for Economic Affairs and Climate Action (BMWK) under Grant No. 50WM2261B. We further thank SpaceTech GmbH (STI) for providing support with the magnet.

AUTHOR DECLARATIONS

Conflict of Interest

The authors have no conflicts to disclose.

Author Contributions

Christoph Tyborski: Conceptualization (equal); Data curation (equal); Investigation (equal); Methodology (equal); Project administration (equal); Supervision (equal); Validation (equal); Visualization (equal); Writing – original draft (equal); Writing – review & editing (equal). **Muhammad T. Hassan**: Investigation (equal); Writing – review & editing (equal). **Thomas Flisgen**: Methodology (equal); Writing – review & editing (equal). **Max Schiemangk**: Conceptualization (equal); Funding acquisition (equal); Methodology (equal); Supervision (equal); Writing – review & editing (equal). **Andreas Wicht**: Conceptualization (equal); Funding acquisition (equal); Methodology (equal); Supervision (equal); Writing – review & editing (equal).

DATA AVAILABILITY

The data that support the findings of this study are available within the article and its supplementary material.

REFERENCES

[1] D. Becker, M. D. Lachmann, S. T. Seidel, H. Ahlers, A. N. Dinkelaker, J. Grosse, O. Hellmig, H. Müntinga, V. Schkolnik, T. Wendrich, A. Wenzlawski, B. Weps, R. Corgier, T. Franz, N. Gaaloul, W. Herr, D. Lüdtke, M. Popp, S. Amri, H. Duncker, M. Erbe, A. Kohfeldt, A. Kubelka-Lange, C. Braxmaier, E. Charron, W. Ertmer, M. Krutzik, C. Lämmerzahl, A. Peters, W. P. Schleich, K. Sengstock, R. Walser, A. Wicht, P. Windpassinger, and E. M. Rasel, Nature **562**, 391–395 (2018).

[2] K. W. Martin, G. Phelps, N. D. Lemke, M. S. Bigelow, B. Stuhl, M. Wojcik, M. Holt, I. Coddington, M. W. Bishop, and J. H. Burke, Phys. Rev. Appl. **9**, 014019 (2018).

[3] H. Müntinga, H. Ahlers, M. Krutzik, A. Wenzlawski, S. Arnold, D. Becker, K. Bongs, H. Dittus, H. Duncker, N. Gaaloul, C. Gherasim, E. Giese, C. Grzeschik, T. W. Hänsch, O. Hellmig, W. Herr, S. Herrmann, E. Kajari, S. Kleinert, C. Lämmerzahl, W. Lewoczko-Adamczyk, J. Malcolm, N. Meyer, R. Nolte, A. Peters, M. Popp, J. Reichel, A. Roura, J. Rudolph, M. Schiemangk, M. Schneider, S. T. Seidel, K. Sengstock, V. Tamma, T. Valenzuela, A. Vogel, R. Walser, T. Wendrich, P. Windpassinger, W. Zeller, T. van Zoest, W. Ertmer, W. P. Schleich, and E. M. Rasel, Phys. Rev. Lett. **110**, 093602 (2013).

[4] Z. Zhang, M. Kushimoto, T. Sakai, N. Sugiyama, L. J. Schowalter, C. Sasaoka, and H. Amano, Appl. Phys. Express **12**, 124003 (2019).

[5] S. J. Eglash and H. K. Choi, Appl. Phys. Lett. **57**, 1292–1294 (1990).

[6] L. Shterengas, G. L. Belenky, J. G. Kim, and R. U. Martinelli, Semicond. Sci. Technol. **19**, 655–658 (2004).

[7] C. Kuhn, M. Martens, F. Mehnke, J. Enslin, P. Schneider, C. Reich, F. Krueger, J. Rass, J. B. Park, V. Kueller, A. Knauer, T. Wernicke, M. Weyers, and M. Kneissl, J. Phys. D: Appl. Phys. **51**, 415101 (2018).

[8] J. Jeschke, M. Martens, A. Knauer, V. Kueller, U. Zeimer, C. Netzel, C. Kuhn, F. Krueger, C. Reich, T. Wernicke, M. Kneissl, and M. Weyers, IEEE Photonics Technol. Lett. **27**, 1969–1972 (2015).

[9] S. Falke, N. Lemke, C. Grebing, B. Lipphardt, S. Weyers, V. Gerginov, N. Huntemann, C. Hagemann, A. Al-Masoudi, S. Häfner, S. Vogt, U. Sterr, and C. Lisdat, New J. Phys. **16**, 073023 (2014).

[10] R. Le Targat, L. Lorini, Y. Le Coq, M. Zawada, J. Guéna, M. Abgrall, M. Gurov, P. Rosenbusch, D. G. Rovera, B. Nagórny, R. Gartman, P. G. Westergaard, M. E. Tobar, M. Lours, G. Santarelli, A. Clairon, S. Bize, P. Laurent, P. Lemonde, and J. Lodewyck, Nat. Commun. **4**, 2782 (2013).

[11] G. Erbert, F. Bugge, A. Knauer, J. Sebastian, A. Thies, H. Wenzel, M. Weyers, and G. Trankle, IEEE J. Sel. Top. Quantum Electron. **5**, 780–784 (1999).

[12]S. Spießberger, M. Schiemangk, A. Wicht, H. Wenzel, O. Brox, and G. Erbert, J. Lightwave Technol. **28**, 2611–2616 (2010).
[13]R. D. Dupuis, P. D. Dapkus, N. Holonyak, E. A. Rezek, and R. Chin, Appl. Phys. Lett. **32**, 295–297 (1978).
[14]H. Hamada, M. Shono, S. Honda, R. Hiroyama, K. Matsukawa, K. Yodoshi, and T. Yamaguchi, Electron. Lett. **27**, 661–662 (1991).
[15]M. P. Faraday, Phil. Trans. R. Soc. Lond. **136**, 1–20 (1846).
[16]I. M. Boswarva, R. E. Howard, and A. B. Lidiard, Proc. R. Soc. London, Ser. A **269**, 125–141 (1962).
[17]L. M. Roth, Phys. Rev. **133**, A542–A553 (1964).
[18]G. Blume, D. Jedrzejczyk, J. Pohl, D. Feise, A. Sahm, N. Werner, C. Nölleke, P. Leisching, and K. Paschke, Proc. SPIE **10528**, 105280D (2018).
[19]J. E. Geusic and H. E. D. Scovil, Bell Labs Tech. J. **41**, 1371–1397 (1962).
[20]L. J. Aplet and J. W. Carson, Appl. Opt. **3**, 544–545 (1964).
[21]J. K. Furdyna, J. Appl. Phys. **64**, R29–R64 (1988).
[22]D. U. Bartholomew, J. K. Furdyna, and A. K. Ramdas, Phys. Rev. B **34**, 6943–6950 (1986).
[23]J. A. Gaj, R. R. Gałązka, and M. Nawrocki, Solid State Commun. **25**, 193–195 (1978).
[24]Y. Hwang and Y. Um, in *2012 7th International Forum on Strategic Technology (IFOST)* (IEEE, 2012), pp. 1–3.
[25]L. Kowalczyk, A. Mycielski, L. Śniadower, and R. R. Gałązka, Phys. Status Solidi C **1**, 985–988 (2004).
[26]M. A. Butler, Solid State Commun. **62**, 45–47 (1987).
[27]D. W. Schubert, M. M. Kraus, R. Kenklies, C. R. Becker, and R. N. Bicknell-Tassius, Appl. Phys. Lett. **60**, 2192–2194 (1992).
[28]N. Kullendorff and B. Hök, Appl. Phys. Lett. **46**, 1016–1018 (1985).
[29]W. Wu, J. Zhang, L. Wang, J. Min, X. Liang, and X. Wen, Phys. Status Solidi C **13**, 408–412 (2016).
[30]U. N. Roy, O. K. Okobiah, G. S. Camarda, Y. Cui, R. Gul, A. Hossain, G. Yang, S. U. Egarievwe, and R. B. James, AIP Adv. **8**, 105012 (2018).
[31]J. Zhang, W. Jie, L. Luan, T. Wang, and D. Zeng, J. Electron. Mater. **37**, 1158–1162 (2008).
[32]O. S. Babalola, A. E. Bolotnikov, M. Groza, A. Hossain, S. Egarievwe, R. B. James, and A. Burger, J. Cryst. Growth **311**, 3702–3707 (2009).
[33]Y. Du, W. Jie, T. Wang, Y. Xu, L. Yin, P. Yu, and G. Zha, J. Cryst. Growth **318**, 1062–1066 (2011).
[34]U. N. Roy, G. S. Camarda, Y. Cui, R. Gul, A. Hossain, G. Yang, O. K. Okobiah, S. U. Egarievwe, and R. B. James, J. Cryst. Growth **509**, 35–39 (2019).
[35]P. Y. Yu and M. Cardona, *Fundamentals of Semiconductors: Physics and Materials Properties*, 4th ed. (Springer, 2010).
[36]K. H. Kim, A. E. Bolotnikov, G. S. Camarda, G. Yang, A. Hossain, Y. Cui, R. B. James, J. Hong, and S. U. Kim, J. Appl. Phys. **106**, 023706 (2009).
[37]Y. R. Lee and A. K. Ramdas, Solid State Commun. **51**, 861–863 (1984).
[38]O. Slezak, R. Yasuhara, A. Lucianetti, and T. Mocek, Opt. Express **23**, 13641–13647 (2015).
[39]E. G. Víllora, P. Molina, M. Nakamura, K. Shimamura, T. Hatanaka, A. Funaki, and K. Naoe, Appl. Phys. Lett. **99**, 011111 (2011).
[40]D. Vojna, O. Slezák, A. Lucianetti, and T. Mocek, Appl. Sci. **9**, 3160 (2019).